THREE POROUS LAYERED FERROFLUID SQUEEZE FILM WITH A CONVEX PAD STATOR UNDER SLIP AND SQUEEZE VELOCITY EFFECTS

Darshana A Patel[1] & Ramesh C Kataria[*2]

[1]Department of Mathematics and Humanities, Vishwakarma Government Engineering College, Ahmadabad, India

[*2]Department of Mathematics, M.G. Science Institute, Navrangpura, Ahmadabad, India

Abstract:

This paper presents a mathematical model and analysis for a slider bearing consisting of a convex pad stator with three porous layers attached to the slider. As a lubricant, ferrofluid is used. The problem takes into account the influence of slip velocity, as proposed by Sparrow *et al.* [1] and modified by Shah *et al.* [2]. To describe magnetic fluid penetration dynamics through porous media, we have used modified Darcy's law given by Zahn and Rosensweig [3]. Solving the generalized Reynolds equation yields the expression for pressure. The equations for load carrying capacity can then be obtained by using this expression. Non-dimensional pressure, load carrying capacity, friction on the slider, coefficient of friction, and position of the centre of pressure are expressed analytically. A numerical computation is performed and graphical results are presented. The results indicate that a greater field strength or greater inlet to outlet film thickness ratio *a* increases load carrying capacity. Non-dimensional coefficient of friction and friction on the moving slider increase with decreasing inlet-to-outlet film thickness ratio *a* or higher crown ratio. When the film thickness ratio increased, the centre of pressure shifted towards the outlet. After the film thickness ratio *a* reached a particular level, it changed in the direction of the inlet as field strength became larger. However, it shifted towards the inlet when the magnetization parameter increased. When the slip parameter was increased, the non-dimensional load capacity, slider friction, and centre of pressure location all decreased. Overall, it can be said that smaller values of k_1, k_2, k_3, and $k_1 < k_2 < k_3$ yield higher performance.

Keywords: Porous plate, Squeeze velocity, Slip velocity, Squeeze film, Ferrofluid.

Nomenclature

a	h_2/h_1, ratio of inlet to outlet film-thickness
A	Bearing length
B	Bearing breadth
d_1, d_2, d_3	Thickness of upper, middle and lower porous matrix (m)

E Defined in Eq. (43)

f Coefficient of friction

$\bar{f}$ Non-dimensional coefficient of friction as defined in Eq. (49)

F Friction on the slider

$\overline{F}$ Non-dimensional friction on the slider as defined in Eq. (48)

G Defined in Eq. (43)

h Fluid film thickness (m)

$\overline{h}$ Non-dimensional film thickness (h / h_1)

h_1 Outlet film thickness(m)

h_2 Inlet film thickness(m)

$\overline{h}_m$ Non-dimensional minimum film thickness as defined in Eq. (52)

$\dot{h}$ dh / dt, Squeeze velocity (m/s)

$H = |\mathbf{H}|$ Magnetic field Strength (Magnitude of **H**) (A /m)

$\boldsymbol{H}$ Applied magnetic field vector

K Quantity defined in Eq. (13) (A^2 / m^4)

k_1, k_2, k_3 Permeability of the upper, middle and lower porous matrix (m^2)

$\boldsymbol{M}$ Magnetization vector

p Film pressure (N / m^2)

P_1 Fluid pressure in the upper porous matrix (N / m^2)

P_2 Fluid pressure in the middle porous matrix (N / m^2)

P_3 Fluid pressure in the lower porous matrix (N / m^2)

$\boldsymbol{q}$ Fluid velocity vector

Q As defined in Eq. (46)

$s = \alpha / \sqrt{k_1}$ Slip parameter (1 / m)

$\bar{s}$ Non-dimensional slip parameter defined in Eq. (40)

t Time (s)

u, v, w Components of film fluid velocity in x, y and z–directions (m/s)

U Surface velocity of slider (m/s)

$\bar{u}_i, \bar{w}_i$ Darcy's velocity components in the x and z - directions respectively

W Load-carrying capacity (N)

$\overline{W}$ Non-dimensional load-carrying capacity as defined in Eq. (47)

x, y, z Co-ordinates (m)

X Non-dimensional coordinate, $\frac{x}{A}$

$\overline{X}$ Position of Centre of pressure

Y Non-dimensional position of centre of pressure, $\frac{\overline{X}}{A}$

r, θ, z Cylindrical polar co-ordinates

Greek symbols

η Fluid viscosity (N s / m^2)

μ_0 Free space permeability (N / A^2)

α Slip constant

δ Central thickness of convex pad (m)

$\bar{\delta}$ $\frac{\delta}{h_1}$ Non-dimensional crown ratio

τ Stress

ρ Fluid density (N s^2 /m^4)

$\overline{\mu}$ Magnetic susceptibility

μ^* Non-dimensional magnetization parameter as defined in Eq. (40)

ϕ Inclination of H with the x-axis

1. Introduction

A colloidal suspension of ferromagnetic particles or their oxide particles (mostly iron oxide, ferric oxide, etc.) in a carrier liquid that is not conducting, such as water, ethylene glycol, engine oil, or mineral oil, is known as a ferrofluid [4-5] or magnetic nanofluid. Ionic liquids are currently used as carrier liquids because of their low vapour pressure and flammability [6–8]. In order to prevent flocculation, surfactants are added to carrier liquids so that their molecules interact with magnetic particles via their functional groups to form a layer around them. Due to the magnetization of ferromagnetic particles, ferrofluid experiences magnetic body force when an external magnetic field is applied. Also, the fluid's viscosity changes. As the fluid's viscosity increases, its load carrying capacity also increases. In spite of this, the magnetic moments of the particles are randomly oriented, and the fluid behaves like a normal fluid without a magnetic field. A typical composition contains 5% magnetic particles, 10% surfactants, and 85% carrier liquids. It is possible to retain ferrofluids at a desired location. There is no chance of side leakage either. This makes ferrofluids useful in a variety of applications [9-13]. A few examples are magnetic seals, rotary seals in computer hard drives, computer hardware, electronic packaging, sensors, aerospace, dynamic loudspeakers, and bioengineering. Recent studies have demonstrated the controllability and positioning properties of ferrofluids as lubricants in hydrodynamic bearings.

For viscous fluids, no-slip boundary conditions mean that when fluid flows over a solid surface, the fluid elements adjacent to the surface reach the surface's velocity. In other words, the no-slip boundary condition assumes that the fluid near to the surface has zero velocity when the surface

is at rest and the fluid velocity equals to the surface velocity when the surface moves. The physical interpretation for the no-slip boundary condition is that the fluid molecules hitting the solid wall collide so frequently with the solid wall molecules that they have no average motion that is different from the wall molecules. The effect of ferrofluid on a porous inclined slider bearing was discussed by Agrawal [14]. It was concluded that magnetization of the magnetic particles in the lubricant enhanced load carrying capacity without affecting friction on moving slider. Characteristics of a double-porous layered slider bearing having a hyperbolic pad stator under the effects of slip and squeeze velocity have been analyzed by Patel and Kataria [15]. They found that the non-dimensional load carrying capacity increased when non-dimensional magnetization parameter increased. Using porous squeeze film bearings, Prajapati [16] theoretically investigated magnetic fluid effects. According to the results, the magnetization parameter increased load carrying capacity.

As part of the lubrication problem analysis, a Reynolds-type equation is developed that governs the mean film pressure. Reynolds equation is derived by assuming that no boundary slip occurs at the solid-liquid interface. On a micro-scale, however, the slip of fluid over solid surfaces can be observed. Due to this, the classical Reynolds equation is no longer relevant. Therefore, boundary slip has been considered in the Reynolds equation. Several contributions related to slip velocity have been made to analyze the performance characteristics of various bearings such as the problems in squeeze film bearing by Sparrow *et al*. [1], for the circular disk by Patel [17], slider bearing by Patel and Gupta [18], Salant and Fortier [19],Wu *et al*. [20], Shah and Bhat [21], and Ahmad and Singh[22], the radial sleeve bearing by Wang *et al*. [23], and infinitely long bearing by Patel and Deheri [24]. Ferrofluid lubricated differently designed bearings have been theoretically studied by Shah *et al*. [25–30], including porous slider bearings of various shapes, long journal bearing, axially undefined journal bearing characterized by slip velocity at the porous boundary and anisotropic permeability of the porous matrix attached to the impermeable plate. Chi *et al*. [32] presented a journal bearing with three pads filled with ferrofluid. There was one that was deformable elastic. This bearing performed much better than ordinary bearings based on the theoretical study and experimental investigation. Also, the bearing was leak-free and operated without any feed system. A ferrofluid-based slider bearing with a parabolic pad stator and two porous thin layers attached to a lower porous plate and an external magnetic field applied obliquely to the lower surface was discussed by Patel and Kataria [33]. According to their findings, load carrying capacity increased with increased magnetization, while slip parameter decreased.

In the best of the authors' knowledge, no research has been conducted to examine the performance of slider bearings with three porous layers attached to the lower plate and convex pad stator, slip and squeeze velocity are taken into consideration. The flow of ferrofluid lubricant is described by a Neuringer-Rosensweig model. As a result, this study attempts to investigate the same. Squeeze and slip velocity are taken into account at the film-porous interface. A

number of variables were evaluated, including non-dimensional pressure, load carrying capacity, friction on the slider, coefficient of friction, and the position of the center of pressure.

2. Equations for generalized ferrofluid lubrication

For governing ferrofluid, Neuringer and Rosensweig proposed a system of equations. This model considers magnetic forces within the body as its main feature. According to the Neuringer-Rosensweig model with continuity equation in cylindrical polar coordinates (r, θ, z) ,ferrofluid motion is described by the following equations for the film region based on ferrohydrodynamic theory

Equation of Motion

$$\rho\left[\frac{\partial \mathbf{q}}{\partial t}+(\mathbf{q}\bullet\nabla)\mathbf{q}\right]=-\nabla p+\eta\nabla^2\mathbf{q}+\mu_0(\mathbf{M}\bullet\nabla)\mathbf{H} \tag{1}$$

Continuity equation for incompressible fluids

$$\nabla\bullet\mathbf{q}=0, \tag{2}$$

Maxwell equations for electrically non-conducting fluid

$$\nabla\times\mathbf{H}=0,\ \mathbf{H}=\nabla\phi,\ \phi=\phi(x,\ z) \tag{3}$$

$$\mathbf{M}=\overline{\mu}\,\mathbf{H} \tag{4}$$

$$\nabla\bullet(\mathbf{H}+\mathbf{M})=0. \tag{5}$$

where η is the fluid viscosity, p is the film pressure, ρ is the fluid density, $\overline{\mu}$ is the magnetic susceptibility, $\overline{\mu}_0$ is the initial susceptibility of fluid, μ_0 is the permeability of free space, $\mathbf{q}$ is the fluid velocity vector, $\mathbf{H}$ is the applied magnetic field vector, $\mathbf{M}$ is the magnetization vector, M is the magnitude of the magnetization vector.

Also,

$$\mathbf{q}=u\mathbf{i}+v\mathbf{j}+w\mathbf{k},$$

where, components of film fluid velocity are represented by *u*, *v*, and *w* in the x, y, and z-directions.

If the direction of fluid element's magnetization is always in the direction of the local magnetic field [28] *i. e.* $\mathbf{M}=\overline{\mu}\,\mathbf{H}$.

As a result, the last term in equation (1) is

$$\mu_0(\mathbf{M}\bullet\nabla)\mathbf{H} = \mu_0\,\bar{\mu}\,(\mathbf{H}\bullet\nabla)\mathbf{H}$$

(6)

Using vector identity $(\mathbf{H}\bullet\nabla)\mathbf{H} = \frac{\mathbf{1}}{\mathbf{2}}\nabla(\mathbf{H}\bullet\mathbf{H}) - \mathbf{H}\times(\nabla\times\mathbf{H})$

(7)

Therefore, equation (6) can be written as

$$\mu_0(\mathbf{M}\bullet\nabla)\mathbf{H} = \mu_0\,\bar{\mu}\,(\mathbf{H}\bullet\nabla)\mathbf{H} = \mu_0\,\bar{\mu}\frac{1}{2}\nabla(\mathbf{H}\bullet\mathbf{H}) = \frac{1}{2}\mu_0\,\bar{\mu}\nabla(\mathrm{H}^2)$$

(8)

Using equation (8) equation (1) becomes

$$\rho\left[\frac{\partial\mathbf{q}}{\partial t} + (\mathbf{q}.\nabla)\mathbf{q}\right] = -\nabla\left(\mathrm{p} - \frac{1}{2}\mu_0\bar{\mu}H^2\right) + \eta\nabla^2\mathbf{q}$$

(9)

In the Navier-Stokes equation, extra pressure $\frac{1}{2}\mu_0\,\bar{\mu}\nabla(\mathrm{H}^2)$ is introduced when magnetic fluid is introduced.

3.Formulation of the problem and its solution

An illustration of a slider bearing with a convex pad stator and central thickness δ is shown in figure 1. The lower surface has a length *A* and moves uniformly in the x-direction at a velocity *U*. Three thin layers make up the lower surface. Porous matrix of first thickness d_3 has been fitted to the slider, followed by d_2 and d_1.

In the present study, the flow is assumed to be laminar, inertia terms are ignored, velocity derivatives across a film are dominant, fluid is incompressible, flow in the film region is axisymmetric, and other usual assumptions about lubrication are assumed to be true.

To describe the pressure distribution *p* in x-direction considering cylindrical coordinates under the above assumptions and using equations (1) to (5), the result [28, 36] is

$$\frac{\partial^2 u}{\partial z^2} = \frac{1}{\eta}\frac{\partial}{\partial x}\left(p - \frac{1}{2}\mu_0\bar{\mu}H^2\right).$$

(10)

A uniform velocity $\dot{h} = \frac{dh}{dt}$

(11)

where *t* is the time, is applied to the stator as it moves towards the slider.
Based on Shah [36, 37 and 38], film thickness h is as follows:

$$h=\delta\left\{4\left(\frac{x}{A}-\frac{1}{2}\right)^2-1\right\}+h_1\left\{a-\frac{a}{A}x+\frac{x}{A}\right\};\quad a=\frac{h_2}{h_1},\ 0\le x\le A \tag{12}$$

Here, maximum and minimum film thicknesses are defined as h_2 and h_1 respectively.

The magnitude *H* of the external magnetic field **H** is expressed as

$$\mathbf{H}=H(\cos\phi(x,z),\ 0,\ \sin\phi(x,z))\ .$$

In this case, the magnetic field *H* is defined as [27]

$$H^2=Kx(A-x), \tag{13}$$

which is oblique to the lower surface. At $x=A/2$, it reaches its maximum. It disappears at the bearing's inlet and outlet. The constant *K* here is chosen to suit the dimensions of both sides.

The shear stress relation is $\tau=\eta\dfrac{\partial u}{\partial z}$ if τ is the stress and *u* is the fluid velocity in the x-direction.

3.1 Continuity equation

For film region

$$\frac{\partial u}{\partial x}+\frac{\partial w}{\partial z}=0 \tag{14}$$

For porous region

$$\frac{\partial \overline{u}}{\partial x}+\frac{\partial \overline{w}}{\partial z}=0 \tag{15}$$

3.2 Darcy's law for the porous region

Additionally, to film flow, bearing material pores also experience flow. Porous matrix is assumed to be homogeneous and isotropic, velocities are continuous between porous layer and film regions, and flow is axisymmetric within the film and porous area. According to modified Darcy's law [3, 35], magnetic fluid in a porous matrix flows as follows:

$$\overline{u}_i=\frac{-k_i}{\eta}\frac{\partial}{\partial x}\left(P_i-\frac{1}{2}\mu_0\overline{\mu}H^2\right),\ (x-\text{direction}) \tag{16}$$

$$\overline{w}_i=\frac{-k_i}{\eta}\frac{\partial}{\partial z}\left(P_i-\frac{1}{2}\mu_0\overline{\mu}H^2\right),\ (z-\text{direction}) \tag{17}$$

Where i =1, 2, 3 indicates the velocity components in a porous matrix with thicknesses d_1, d_2, and d_3. Further, k_1, k_2 and k_3 represent the permeabilities in the upper, middle, and lower layers of the porous matrix.

Under boundary conditions [1, 27],

$$u = 0 \quad \text{when } z = h$$
$$u = \frac{1}{s}\frac{\partial u}{\partial z} + U \quad \text{when } z = 0,\ s = \frac{\alpha}{(k_1)^{1/2}} \tag{18}$$

And by integrating equation (10) twice with respect to z, one can find

$$u = \frac{s(h-z)}{(1+sh)}U + \left\{\frac{((1+sh)z+h)(z-h))}{2\eta\ (1+sh)}\right\}\frac{\partial}{\partial x}\left(p - \frac{1}{2}\mu_0\bar{\mu}H^2\right), \tag{19}$$

Here s stands for slip constant, α for slip coefficient, and k_1 for permeability of the upper porous layer. These all depend on the properties of the porous material and are independent of the lubricant's properties and film thickness. On the x-axis, U represents uniform sliding velocity component.

By integrating continuity equation (14) over film thickness (0, h) and using equation (19), we obtain

$$\frac{\partial}{\partial x}\left\{\frac{sh^2}{2(1+sh)}U - \frac{h^3(4+sh)}{12\eta(1+sh)}\frac{\partial}{\partial x}\left(p - \frac{1}{2}\mu_0\bar{\mu}H^2\right)\right\} = w_0 - V, \tag{20}$$

In this case, $w|_{z=h} = w_h = V = -\dot{h}$, represents the downward z -direction squeeze velocity. And

$$w|_{z=0} = w_0 . \tag{21}$$

When Eq.s (16) and (17) are applied to the continuity Eq. (15) of porous region, we are able to find

$$\frac{\partial^2}{\partial x^2}\left(P_i - \frac{1}{2}\mu_0\bar{\mu}H^2\right) + \frac{\partial^2}{\partial z^2}\left(P_i - \frac{1}{2}\mu_0\bar{\mu}H^2\right) = 0, \quad i = 1,\ 2,\ 3 \tag{22}$$

Boundary conditions

In the case under consideration, the boundary conditions are as follows:

$$p(x) = P_1(x,\ 0) \tag{23}$$

$$P_1(x, -d_1) = P_2(x, -d_1)$$

(24)

$$P_2\left(x,-(d_1+d_2)\right)= P_3\left(x, -(d_1+d_2)\right)$$

(25)

$$\left[k_1\frac{\partial}{\partial z}\left(P_1-\frac{1}{2}\mu_0\bar{\mu}H^2\right)\right]_{z=-d_1}=\left[k_2\frac{\partial}{\partial z}\left(P_2-\frac{1}{2}\mu_0\bar{\mu}H^2\right)\right]_{z=-d_1}$$

(26)

$$\left[k_2\frac{\partial}{\partial z}\left(P_2-\frac{1}{2}\mu_0\bar{\mu}H^2\right)\right]_{z=-(d_1+d_2)}=\left[k_3\frac{\partial}{\partial z}\left(P_3-\frac{1}{2}\mu_0\bar{\mu}H^2\right)\right]_{z=-(d_1+d_2)}$$

(27)

$$\left(\frac{\partial}{\partial z}\left(P_3-\frac{1}{2}\mu_0\bar{\mu}H^2\right)\right)_{z=-(d_1+d_2+d_3)}=0 \quad .$$

(28)

Eq. (23) is a result of continuous pressure at the interface between the oil film and the inner layer of the porous bearing. Two porous layers are connected by continuity of pressure in Eq.s (24) and (25) respectively. The impervious boundary does not permit flow, as indicated by Eq. (28).In Eq.s (26) and (27) we assume that the flow normal to the boundary between the two porous layers is equal on both sides.

By integrating Eq. (22) with respect to z over the porous layer of thickness d_1, we find

$$\frac{\partial}{\partial z}\left(P_1-\frac{1}{2}\mu_0\bar{\mu}H^2\right)\Big|_{z=0}=-\int_{-d_1}^{0}\frac{\partial^2}{\partial x^2}(P_1-\frac{1}{2}\mu_0\bar{\mu}H^2)dz+\frac{\partial}{\partial z}\left(P_1-\frac{1}{2}\mu_0\bar{\mu}H^2\right)\Big|_{z=-d_1} .$$

(29)

From condition (26), Eq. (29) reduces to

$$\frac{\partial}{\partial z}\left(P_1-\frac{1}{2}\mu_0\bar{\mu}H^2\right)\Big|_{z=0}=-\int_{-d_1}^{0}\frac{\partial^2}{\partial x^2}(P_1-\frac{1}{2}\mu_0\bar{\mu}H^2)dz+\frac{k_2}{k_1}\frac{\partial}{\partial z}\left(P_2-\frac{1}{2}\mu_0\bar{\mu}H^2\right)\Big|_{z=-d_1} \quad (30)$$

From condition (27), by integrating Eq. (22) with respect to z over the porous layer of thickness d_2, we obtain

$$\frac{\partial}{\partial z}\left(P_2-\frac{1}{2}\mu_0\bar{\mu}H^2\right)\Big|_{z=-d_1}=-\int_{-(d_1+d_2)}^{-d_1}\frac{\partial^2}{\partial x^2}(P_2-\frac{1}{2}\mu_0\bar{\mu}H^2)dz+\frac{\partial}{\partial z}\left(P_2-\frac{1}{2}\mu_0\bar{\mu}H^2\right)\Big|_{z=-(d_1+d_2)}$$

(31) reduces to

$$\frac{\partial}{\partial z}\left(P_2-\frac{1}{2}\mu_0\bar{\mu}H^2\right)\Big|_{z=-d_1}=-\int_{-(d_1+d_2)}^{-d_1}\frac{\partial^2}{\partial x^2}(P_2-\frac{1}{2}\mu_0\bar{\mu}H^2)dz+\frac{k_3}{k_2}\frac{\partial}{\partial z}\left(P_3-\frac{1}{2}\mu_0\bar{\mu}H^2\right)\Big|_{z=-(d_1+d_2)}$$

(32)

Eq. (30) and (32) give us

$$\frac{\partial}{\partial z}\left(P_1-\frac{1}{2}\mu_0\bar{\mu}H^2\right)\Big|_{z=0}=-\int_{-d_1}^{0}\frac{\partial^2}{\partial x^2}(P_1-\frac{1}{2}\mu_0\bar{\mu}H^2)dz+\frac{k_3}{k_1}\frac{\partial}{\partial z}\left(P_3-\frac{1}{2}\mu_0\bar{\mu}H^2\right)\Big|_{z=-(d_1+d_2)}$$
$$-\frac{k_2}{k_1}\int_{-(d_1+d_2)}^{-d_1}\frac{\partial^2}{\partial x^2}\left(P_2-\frac{1}{2}\mu_0\bar{\mu}H^2\right)dz \quad (33)$$

As a result of integrating Eq. (22) with respect to z over the porous layer of thickness d_3, we obtain

$$\frac{\partial}{\partial z}\left(P_3-\frac{1}{2}\mu_0\bar{\mu}H^2\right)\Big|_{z=-(d_1+d_2)}=-\int_{-(d_1+d_2+d_3)}^{-(d_1+d_2)}\frac{\partial^2}{\partial x^2}(P_3-\frac{1}{2}\mu_0\bar{\mu}H^2)dz \quad (34)$$

Due to the porous facing being pressed into an impermeable housing, $\frac{\partial}{\partial z}\left(P_3-\frac{1}{2}\mu_0\bar{\mu}H^2\right)$ at $z=-(d_1+d_2+d_3)$ is zero.

By using Eq. (34) Eq. (33) becomes

$$\frac{\partial}{\partial z}\left(P_1-\frac{1}{2}\mu_0\bar{\mu}H^2\right)\Big|_{z=0}=-\int_{-d_1}^{0}\frac{\partial^2}{\partial x^2}(P_1-\frac{1}{2}\mu_0\bar{\mu}H^2)dz-\frac{k_2}{k_1}\int_{-(d_1+d_2)}^{-d_1}\frac{\partial^2}{\partial x^2}\left(P_2-\frac{1}{2}\mu_0\bar{\mu}H^2\right)dz$$
$$-\frac{k_3}{k_1}\int_{-(d_1+d_2+d_3)}^{-(d_1+d_2)}\frac{\partial^2}{\partial x^2}\left(P_3-\frac{1}{2}\mu_0\bar{\mu}H^2\right)dz. \quad (35)$$

When considering a thin wall, Eq. (35) can be simplified to Eq.

$$\frac{\partial}{\partial z}\left(P_1-\frac{1}{2}\mu_0\bar{\mu}H^2\right)\Big|_{z=0}=-\left(d_1+\frac{k_2}{k_1}d_2+\frac{k_3}{k_1}d_3\right)\frac{\partial^2}{\partial x^2}\left(P-\frac{1}{2}\mu_0\bar{\mu}H^2\right) \quad (36)$$

using the Morgan-Cameron approximation [35].

Due to the continuity of the fluid velocity components across the surface $z=0$

$$w\big|_{z=0}=\overline{w}_1\big|_{z=0} \quad (37)$$

Using Eq. (20) and Eq. (16) at z = 0, Eq. (37) becomes

$$\frac{\partial}{\partial x}\left\{\frac{sh^2}{2(1+sh)}U-\frac{h^3(4+sh)}{12\eta(1+sh)}\frac{\partial}{\partial x}\left(p-\frac{1}{2}\mu_0\bar{\mu}H^2\right)\right\}-\dot{h}=\left[\frac{-k_1}{\eta}\frac{\partial}{\partial z}\left(P_1-\frac{1}{2}\mu_0\bar{\mu}H^2\right)\right]\Big|_{z=0} \quad (38)$$

By using Eq. (36) and the fact that $\frac{\partial H^2}{\partial z}=0$ Eq. (38) becomes

$$\frac{d}{dx}\left\{\left\{12k_1\left(d_1+\frac{k_2}{k_1}d_2+\frac{k_3}{k_1}d_3\right)+\frac{h^3(4+sh)}{(1+sh)}\right\}\frac{d}{dx}\left(p-\frac{1}{2}\mu_0\bar{\mu}H^2\right)\right\}=12\eta V+6\eta U\frac{d}{dx}\left(\frac{sh^2}{1+sh}\right)$$

(39)

represents Reynolds's equation of the governing phenomenon.
Non-dimensional quantities defined as

$$X=\frac{x}{A},\ \bar{h}=\frac{h}{h_1},\ \bar{s}=sh_1,\ a=\frac{h_2}{h_1},\ \bar{p}=\frac{h_1^2 p}{\eta UA},\ \bar{\delta}=\frac{\delta}{h_1},\mu^*=\frac{\mu_0\bar{\mu}KAh_1^2}{\eta U},\ \psi=\frac{k_1d_1+k_2d_2+k_3d_3}{h_1^3},\ S=\frac{-2VA}{Uh_1}$$

(40)

As a result of Eq. (13), we have the magnetic field

$$H^2=KA^2X(1-X),$$

(41)

And the Eq. (38) becomes

$$\frac{d}{dX}\left[G\frac{d}{dX}\left\{\bar{p}-\frac{1}{2}\mu^*X(1-X)\right\}\right]=\frac{dE}{dX},$$

(42)

Where $G=12\psi+\frac{\bar{h}^3(4+\bar{s}\bar{h})}{(1+\bar{s}\bar{h})},\ E=\frac{6\bar{s}\bar{h}^2}{(1+\bar{s}\bar{h})}-6SX.$

(43)

Film thickness can be expressed [37, 38] as

$$\bar{h}=4\bar{\delta}X^2-(a-1+4\bar{\delta})X+a,\ 0\le X\le 1$$ in its non-dimensional form.

(44)

Reynold's Eq. (42) is a non-dimensional version.

4. Solution of the problem

Solution of Eq. (42) with boundary conditions

$$\bar{p}=0,$$ when X = 0, 1.

(45)

yields $\bar{p}=\frac{1}{2}\mu^*X(1-X)+\int_0^X\frac{E-Q}{G}dX,$ where $Q=\frac{\int_0^1\frac{E}{G}dX}{\int_0^1\frac{1}{G}dX}.$

(46)

Using non-dimensional terms, the load carrying capacity W of the bearing can be expressed as follows [27]

$$\bar{W}=\int_0^1\bar{p}\ dX,\ \text{where}\ \bar{W}=\frac{W h_1^2}{A^2B\eta U},$$

Using Eq. (46), the non-dimensional form

$$\bar{W} = \frac{W h_1^2}{A^2 B \eta U} = \frac{\mu^*}{12} - \int_0^1 \frac{E-Q}{G} X \, dX. \tag{47}$$

Friction F on the slider can be obtained as

$$F = \int_0^A \int_0^B \eta \left. \frac{\partial u}{\partial z} \right|_{z=0} dx \, dy$$

Friction on the slider takes the non-dimensional form as

$$\bar{F} = \frac{-h_1 F}{AB\eta U} = \int_0^1 \left(\frac{\bar{s}\,\bar{h}^2 (E-Q)}{2G(1+\bar{s}\bar{h})} + \frac{\bar{s}}{(1+\bar{s}\bar{h})} \right) dX. \tag{48}$$

And coefficient of friction f is given by $f = \frac{F}{W}$.

The non-dimensional form of coefficient of friction takes the form

$$\bar{f} = \frac{-Af}{h_1} = \frac{\bar{F}}{\bar{W}}. \tag{49}$$

The position of the centre of pressure $\bar{X}$ can be determined as follows

$$\bar{X} = \frac{1}{W} \int_0^A \int_0^B p \, x \, dx \, dy$$

and the non-dimensional form of the position of the center of pressure is given by

$$Y = \frac{\bar{X}}{A} = \frac{1}{\bar{W}} \left[\frac{\mu^*}{24} - \frac{1}{2} \int_0^1 X^2 \left(\frac{E-Q}{G} \right) dX \right] \tag{50}$$

B represents the breadth of the bearing with $A << B$.

Minimum film thickness

In general, the minimum film thickness for a flat pad surface is equal to the outlet film thickness h_1, but it is not equal for convex pads. In the case of convex pads, the minimum film thickness depends on the maximum height of the crown segments and inclination of the pad. This may be obtained by differentiating Eq. (44) with respect to X and equating to zero as follows

$$\frac{dh}{dX} = 0 \;\Rightarrow X = \frac{a-1}{8\bar{\delta}} + \frac{1}{2}, \;\; \bar{\delta} = \frac{\delta}{h_1} \tag{51}$$

Substituting value of X in Eq. (44) gives non-dimensional form of minimum film thickness $\bar{h}_m$ as [38]

$$\bar{h}_m = \left(\frac{a+1}{2} - \frac{(a-1)^2}{16\bar{\delta}} - \bar{\delta} \right). \tag{52}$$

5. Results and Discussion

For designing the slider bearing with three porous layers attached to the slider and convex pad stator using ferrofluid as a lubricant, Eq.s (46) to (50) determine the important characteristics such as non-dimensional pressure, load carrying capacity, friction on the slider, coefficient of friction, and position of center of pressure.

Based on the following analysis, it is concluded that slip velocity, squeeze velocity, magnetization, and ferrofluid as a lubricant contribute adequately to the bearing's design requirements.

Unless specified, the following representative values are taken in calculations and remain fixed throughout the calculation [36, 38].

$h_1 = 0.05(m),\ h_2 = 0.10(m),\ \bar{\mu} = 0.05,\ U = 1\ (ms^{-1}),\ A = 0.15\ (m),\ \eta = 0.012\ (kg\,m^{-1}s^{-1}),$
$\mu_0 = 4\pi \times 10^{-7}(kg\,m\,s^{-2}\,A^{-2}),\ \delta = 0.015(m),\ \dot{h} = -0.005\ (ms^{-1}),\ d_1 = 0.05(m),\ d_2 = 0.05(m),\ d_3 = 0.05(m),$
$K = 10^8 / 0.56,\ \alpha = 0.1.$

For the above values of the parameters, Simpson's 1/3 rule with a step size of 0.1 has been used to calculate non-dimensional load carrying capacity $\bar{W}$, friction on the slider $\bar{F}$, and coefficient of friction $\bar{f}$, position of centre of pressure *Y*.

Verma [31] published an interesting parallel work recently. The study about ferrofluid lubricated squeeze film between two approaching surfaces. The lower surface consisting of three thin layers, while the top surface is a rigid rectangular smooth plate. This article, however, describes a slider bearing with three porous layers attached to a convex pad stator.

Figure 2 shows the order of magnetic field strength *O*(*H*) for different *K* values when A= 0.15 (m). *K* (for fixed *A*) determines the largest value of magnetic field strength, and as *K* increases, *O* (H) increases.

In Figure 3, a bell-shaped (normal) curve is depicted for the variation in non-dimensional film pressure for different values of non-dimensional parameter *X* using different values of *K* considering $\bar{\delta} = 0.6$ and $k_1 = k_2 = k_3 = 0.0001$. It shows that $\bar{p}$ significantly increases for increasing values of the field strength *K*. From the total pressure generation in the interval $0 \le X \le 1.0$, it is observed that the maximum generation occurs approximately in the interval $0.2 \le X \le 0.8$ for $K = 10^{10} / 0.56$ and $10^9 / 0.56$. This behavior of $\bar{p}$ agrees with those of references [33, 37].

Based on the non-dimensional coordinate *X* = 0.2, 0.4, 0.6, 0.8 and 1.0. Figure 4 shows the effect of the permeability parameter ψ on the non-dimensional film pressure $\bar{p}$ taking into account $\bar{\delta} = 0.6$ and $k_1 = k_2 = k_3 = 0.0001$. It has been observed that as the permeability parameter ψ

increases, the non-dimensional film pressure $\bar{p}$ declines. In addition, it peaks at X = 0.8. Further, $\bar{p}$ takes significantly higher and notable values for $\psi = 0.1$ than $\psi = 1.0$. The following physical process can be used to interpret this declining tendency: According to [1], the fluid can easily exit the bearing environment due to the pressure in porous media The greater the permeability, the easier it is for fluids to pass through the porous material. As a result, the porous material's presence reduces the resistance to flow in the x-direction, which in turn lowers the film pressure. Therefore, the porosity of the porous matrix should be at an optimum level that does not significantly affect bearing pressure.

Table 1 $\bar{p}$ verses $\bar{\delta}$ for various values of X considering $K = \frac{10^8}{0.56}$.

$\bar{\delta}$	$\bar{p}$				
	X = 0.1	X = 0.3	X = 0.5	X = 0.7	X = 0.9
1.2	0.0431536	0.1031293	0.1331427	0.1400051	0.1276650
0.6	0.0286205	0.0853938	0.1269460	0.1472750	0.1465625
0.3	0.0044867	0.0190134	0.0398608	0.0586827	0.0669104

For different values of X, table 1 and Figure 5 present values of $\bar{p}$ with non-dimensional parameter $\bar{\delta}$ taking into account $k_1 = k_2 = k_3 = 0.0001$. The effect of $\bar{\delta}$ on $\bar{p}$ has been observed.

Table 2 $\bar{p}$ verses $\bar{\delta}$ for various values of a

$\bar{\delta}$	$\bar{p}$				
	a =1.8	a =1.9	a =2.0	a =2.1	a =2.2
1.2	0.1141683	0.1146258	0.1150024	0.1152964	0.1155060
0.9	0.1327885	0.1322889	0.1316466	0.1308600	0.1299268
0.6	0.1454815	0.1423144	0.1388049	0.1349280	0.1342120
0.3	0.1022075	0.0849407	0.0653403	0.043026	0.0175412

Table 2 presents values of $\bar{p}$ with non-dimensional parameter $\bar{\delta}$ for different values of a considering X=1.0 and $k_1 = k_2 = k_3 = 0.0001$. It is observed that $\bar{p}$ is affected by $\bar{\delta}$. $\bar{p}$ reaches its maximum value at $\bar{\delta} = 0.6$. In addition, for $\bar{\delta} = 0.9, 0.6 \text{ and } 0.3$, $\bar{p}$ decreases with increasing a, but for $\bar{\delta} = 1.2$, it reverses this trend.

Table 3 Effects on $\overline{W}$ for the same values of k_1, k_2 and k_3

k_1	k_2	k_3	$\overline{W}$					
			$\dot{h}=0$		Due to ferrofluid's use as lubricant, $\overline{W}$ increased by a percentage	$\dot{h}\neq 0$		Due to ferrofluids use as lubricant, $\overline{W}$ increased by a percentage
			$\mu^*=0$	$\mu^*\neq 0$		$\mu^*=0$	$\mu^*\neq 0$	
0.0001	0.0001	0.0001	0.0329291	0.0621595	88.77	0.0347284	0.0639588	84.17
0.01	0.01	0.01	0.0003927	0.0296231	7443.44	0.0004888	0.0297192	5980.03
Percentage increase in $\overline{W}$			8285.31	109.83		7004.83	115.21	

By taking into account the identical values of k_1, k_2 and k_3 and assuming $\dot{h}=0$ and $\dot{h}\neq 0$, Table 3 analyses the effects of conventional lubricant and magnetic fluid on non-dimensional load carrying capacity $\overline{W}$. It has been revealed that the performance of magnetic fluid as lubricant increases more than that of traditional lubricant. When $\mu^*\neq 0$, $\overline{W}$ increases about 88.77 % for $\dot{h}=0$ and 84.17 % for $\dot{h}\neq 0$ as compared to $\mu^*=0$ considering $k_1=k_2=k_3=$ 0.0001. Additionally, it is noted that $\overline{W}$ has a considerably higher value in the case of $k_1=k_2=k_3$ =0.0001 than $k_1=k_2=k_3$ =0.01.

Table 4 Effects of switching the values of k_1 and k_3 on $\overline{W}$

			$\overline{W}$	
k_1	k_2	k_3	$\dot{h}=0$	$\dot{h}\neq 0$
0.0001	0.001	0.01	0.0343358	0.0345790
0.01	0.001	0.0001	0.0301528	0.0303836
Percentage increase in $\overline{W}$			13.87	13.80

For two distinct situations of $\dot{h}=0$ and $\dot{h}\neq 0$, Table 4 shows the values of $\overline{W}$ by switching the values of k_1 and k_3 and keeping $k_2=0.001$ fixed. When $k_1<k_2<k_3$ compared to $k_1>k_2>k_3$, it is seen that $\overline{W}$ grows by roughly 13.87% for $\dot{h}=0$ and 13.80% for $\dot{h}\neq 0$.

Table 5 Effects of switching the values of k_2 and k_3 on $\overline{W}$

			$\overline{W}$	
k_1	k_2	k_3	$\dot{h}=0$	$\dot{h}\neq 0$
0.1	0.1	0.0001	0.0292521	0.0292675
0.1	0.0001	0.1	0.0292521	0.0292675

Table 5 presents the values of $\overline{W}$ by interchanging the values of k_2 and k_3 keeping $k_1 = 0.1$ fixed for two different cases of $\dot{h}=0$ and $\dot{h}\neq 0$. Table 5 shows that while $k_1 = 0.1$ is fixed, the non-dimensional load carrying capacity $\overline{W}$ for both $k_2 > k_3$ and $k_3 > k_2$ remains the same.

Table 6 Effects of switching the values of k_1 and k_2 on $\overline{W}$

			$\overline{W}$	
k_1	k_2	k_3	$\dot{h}=0$	$\dot{h}\neq 0$
0.0001	0.1	0.1	0.0295626	0.0295781
0.1	0.0001	0.1	0.0292521	0.0292675
Percentage increase in $\overline{W}$			1.06	1.06

Table 6 provides the values $\overline{W}$ for two distinct scenarios of $\dot{h}=0$ and $\dot{h}\neq 0$ by switching the values of k_1 and k_2 while keeping $k_3 = 0.1$ constant. It shows that, when $k_3 = 0.1$ held constant, $\overline{W}$ rises by roughly 1.06% for $k_1 < k_2$ compared to $k_1 > k_2$ for both the scenarios.

Figure 6 shows the variation in $\overline{W}$ as a function of non-dimensional parameter *a*, for different non-dimensional parameter *K* considering $k_1 = 0.0001$ and $\psi = 0.1$. It is observed that $\overline{W}$ increases for increasing values of *K* or *a*. It can be significantly increased by increasing *K*. Additionally, the rate of increase of $\overline{W}$ is higher in the case of $K = 10^{10}/0.56$ compared to $K = 0$.

Table 7 Effects on *Y* when k_1 and k_3 are switched over

k_1	k_2	k_3	Y
0.1	0.01	0.001	0.4999370
0.001	0.01	0.1	0.4995306

Table 7 presents the values of Y by interchanging the values of k_1 and k_3 keeping $k_2 = 0.01$ fixed. When $k_1 > k_3$, Y increases about 0.08% as compared to $k_1 < k_3$.

Figure 7 depict the variation in the position of centre of pressure *Y* as a function of the non-dimensional parameter *a*, taking into consideration the non-dimensional parameter *K* fixing $k_1 = 0.0001$ and $\psi = 0.1$. It is shown that as field strength increases, *Y* moves towards the outlet. But shifts towards the inlet when $a > a_1$, $1.8 < a_1 < 1.925$. Additionally, when *a* increase,

the location of the centre of pressure Y moves closer to the outlet. This centre of pressure behavior is consistent with the observations made in the source [37].

In Figure 8, the variation in $\overline{W}$ is shown as a function of the non-dimensional parameter μ^* for various non-dimensional slip parameter $1/\bar{s}$ in consideration of $k_1 = k_2 = k_3 = 0.0001$. It is observed, in general that $\overline{W}$ increases when the slip parameter $1/\bar{s}$ decreases. The reason for this is that slip velocity reduces friction between fluids and boundaries. Furthermore, $\overline{W}$ increases as the magnetization parameter μ^* increases. It may be that magnetization increases the viscosity of the lubricant, which in turn increases pressure and consequently load carrying capacity. Furthermore, Eq. (47), shows an increase in non-dimensional load carrying capacity by $\frac{\mu^*}{12}$ over conventional lubricants. As a result, bearing performance significantly improves when magnetic fluid is present. A similar behavior was found by Shah and Bhat [27].

Figure 9 illustrates the change in Y caused by the non-dimensional magnetization parameter μ^* for various non-dimensional slip parameter $1/\bar{s}$ with $k_1 = k_2 = k_3 = 0.0001$. It shows that for increasing values of $1/\bar{s}$, the centre of pressure Y's location changed towards the outflow edge. Also, as the magnetization parameter μ^* increased, the centre of pressure Y's position also moved in the direction of the inlet. This is consistent with the findings of a theoretical study by Shah and Bhat [27].

When different values of the non-dimensional slip parameter $1/\bar{s}$ are taken into account, Figure 10 illustrates the change in $\overline{F}$ as a function of the non-dimensional magnetization parameter μ^*. It indicates that $\overline{F}$ increases occur with $1/\bar{s}$ decreases. However, increasing μ^*, the friction on the slider did not affect it.

Table 8 Effects on Y, $\overline{F}$ and $\bar{f}$ for interchanging values of k_2 and k_3

k_1	k_2	k_3	Y	$\overline{F}$	$\bar{f}$
0.1	0.1	0.0001	0.4999638	0.0154949	0.5293972
0.1	0.0001	0.1	0.4999638	0.0154949	0.5293972

Table 8 shows the values of Y, $\overline{F}$ and $\bar{f}$ by interchanging the values of k_2 and k_3 keeping $k_1 = 0.1$ fixed. From table 8, it can be shown that Y, $\overline{F}$ and $\bar{f}$ remains fixed when we swapping the values of k_2 and k_3 keeping $k_1 = 0.1$ fixed.

Table 9 $\overline{F}$ verses K for various values of a, allowing for $k_1 = 0.0001$ and $\psi = 0.1$

	$\overline{F}$				
K	a =1.8	a =1.9	a =2.0	a =2.1	a =2.2
0	0.3227891	0.3196558	0.3167365	0.3140092	0.3114539
$10^8/0.56$	0.3227891	0.3196558	0.3167365	0.3140092	0.3114539

$10^9/0.56$	0.3227891	0.3196558	0.3167365	0.3140092	0.3114539
$10^{10}/0.56$	0.3227891	0.3196558	0.3167365	0.3140092	0.3114539

Table 9 shows the values of $\overline{F}$ when *a* = 1.8, 1.9, 2.0, 2.1 and 2.2 for different values of field strength *K*. It is observed from table 9 that $\overline{F}$ decreases when inlet to outlet film thickness ratio *a* increases. Also, percentage increase in $\overline{F}$ is about 3.64 % as inlet to outlet film thickness ratio *a* moves from 1.8 to 2.2. However, $\overline{F}$ remains same as field strength *K* increases.

Table 10 Effects on $\overline{F}$ and $\bar{f}$ for interchanging values of k_1 and k_3

k_1	k_2	k_3	$\overline{F}$	$\bar{f}$
0.0001	0.001	0.01	0.3177271	8.8877258
0.01	0.001	0.0001	0.0470422	1.5480635

Table 10 shows the values of $\overline{F}$ and $\bar{f}$ by switching the values of k_1 and k_3 keeping $k_2 = 0.001$ fixed. From the table 10, it can be seen that when $k_1 < k_2 < k_3$, $\overline{F}$ grows by around 1445.60% and $\bar{f}$ increases by about 1591.22% in comparison to $k_1 > k_2 > k_3$.

Figure 11 depicts variations in $\overline{W}$ as a function of the non-dimensional parameter *a* for various non-dimensional parameters $\overline{\delta}$ .It has been noted that $\overline{W}$ improves as the ratio of in the inlet to outlet film thickness *a* increases. This is due to the fact that ferrofluid produces spikes when a magnetic field is applied, and a spike's ability to transport load carrying capacity may increase because of their strength. Ram *et al.* [39] also reached the same conclusion; hence the findings in the current research serve as confirmation of that conclusion.

The variation of non-dimensional minimum film thickness $\overline{h}_m$ verses non-dimensional parameter *a* under the influence of non-dimensional parameter $\overline{\delta}$ have been observed in Figure 12. It is noted that $\overline{h}_m$ increases as *a* increases. Also, as $\overline{\delta}$ increases $\overline{h}_m$ decreases. This action of concurs with the finding of [39].

Figure 13 illustrates change in $\bar{f}$ as a function of non-dimensional parameter *a*, for various non-dimensional parameter *K*, taking $k_1 = 0.0001$ and $\psi = 0.1$ into account and it is shown that coefficient of friction $\bar{f}$ decreases with increasing values of inlet to outlet film thickness ratio *a* or field strength *K*.

In Figure 14, $\overline{F}$ is plotted versus non-dimensional parameter *a*, for non-dimensional parameter $\overline{\delta}$. It shows that $\overline{F}$ decreases as inlet to outlet ratio *a* increases. In addition, as the non-dimensional crown ratio $\overline{\delta}$ increases, $\overline{F}$ increases as well.

For different non-dimensional parameters $\bar{\delta}$, Figure 15 shows how $\bar{f}$ varies with dimensionless parameter *a*. Based on Figure 15, $\bar{f}$ decreases as inlet to outlet ratio *a* increases. Also, the non-dimensional crown ratio $\bar{\delta}$ increases as $\bar{f}$ increases.

A general overview of the topic is presented here

- If $\mu^* \to 0$ is the case, then the present analysis reduces to non-magnetic lubricants.
- When $s \to 0$, results in a bearing system with no slip at the surface.
- The present analysis reduces to inclined slider bearings when $\delta \to 0$ is present.
- When $\psi \to 0$, the present case reduces to [37] impermeable bearing surface, *i.e.* non-porous slider. Source [37] describes the flow of ferrofluid-lubricated slider bearings with convex pads using Jenkins' model. Here, it was shown that magnetic fluid improves bearing performance. Also, the increases in pressure and load capacity depend only on the field strength. Also, with the increase in film thickness ratio, load capacity increases whereas the friction force on the slider decreases.
- If $d_3 = 0$ is taken into account, the present analysis reduces to source [36]. In this study, we found that smaller values of k_1, k_2 and $k_1 > k_2$. result in better load bearing capacity.

6. Conclusion

Following are the findings from the analysis and results:

1. When the external magnetic fluid's intensity is increased, $\bar{p}$ increases significantly.
2. The permeability parameter ψ increases, $\bar{p}$ declines.
3. When $k_1 < k_2 < k_3$ compared to $k_1 > k_2 > k_3$, it is seen that $\overline{W}$ grows by roughly 13.87% for $\dot{h} = 0$ and 13.80% for $\dot{h} \neq 0$.
4. When $\mu^* \neq 0$, $\overline{W}$ increases about 88.77 % for $\dot{h} = 0$ and 84.17 % for $\dot{h} \neq 0$ as compared to $\mu^* = 0$ considering $k_1 = k_2 = k_3 = 0.0001$. Additionally, it is noted that $\overline{W}$ has a considerably higher value in the case of $k_1 = k_2 = k_3 = 0.0001$ than $k_1 = k_2 = k_3 = 0.01$.
5. $\overline{W}$ remains same for both $k_2 > k_3$ and $k_3 > k_2$ when keeping $k_1 = 0.1$ fixed for both $\dot{h} = 0$ and $\dot{h} \neq 0$. While $k_1 < k_2$ $\overline{W}$ increases about 1.06% as compared to $k_1 > k_2$ keeping $k_3 = 0.1$ fixed.
6. As the value of non-dimensional parameters *K* or the inlet-outlet film thickness ratio *a* increases, $\overline{W}$ also increases.
7. A higher ratio of inlet to outlet film thickness *a* leads to a greater non-dimensional minimum film thickness.
8. As inlet to outlet film thickness ratio *a* decrease or crown ratio increase, non-dimensional friction on the slider and coefficient friction increases. In addition, friction on the slider stays the same with an increase in field strength *K*, whereas coefficient of friction increases with a decrease in field strength *K*.
9. Increases in field strength *K* or the film thickness ratio cause the center of pressure to shift towards the outlet edge, and increases in slip parameter values or magnetization parameter cause it to shift towards the inlet edge.

10. When the slip parameter was increased, the position of centre of pressure, slider friction, and non-dimensional load capacity all went down. However, the magnetization parameter did not affect non-dimensional friction on the slider.

It is thought that bearing design engineers can benefit from the outcomes drawn from the analysis.

Conflict of interest statement

The author states that there are no conflicts of interest

References

1. Sparrow, E. M., Beavers, G. S., & Hwang, I. T. (1972). Effect of velocity slip on porous walled squeeze films. *Journal of lubrication Technology*, 94(3), 260-265.
2. Shah, R.C., & Kataria, R.C. (2016). On the squeeze film characteristics between a sphere and a flat porous plate using ferrofluid. *Applied Mathematical Modeling*, Volume 40, 2473-2484.
3. Zahn, M., & Rosensweig, R. E. (1980). Stability of magnetic fluid penetration through a porous medium with uniform magnetic field oblique to the interface. *IEEE Trans. on Magnetics*, 16(2), 275-282.
4. Rosensweig, R. E. (1985). *Ferrohydrodynamics*. Cambridge University Press.
5. Papell, S. S. (1965). Low viscosity magnetic fluid obtained by the colloidal suspension of magnetic particles. *U. S. Patent* no 3,215,572.
6. Oliveira, F.C.C., Rossi, L. M., Jardim, R. F., & Rubim, J. C. (2009). Magnetic fluids based on γ-Fe2O3 and CoFe2O4 Nanoparticles dispersed in ionic liquids. *The Journal of Physical Chemistry C*, 113(20), 8566–8572.
7. Huang, W. & Wang, X. (2012). Study on the properties and stability of ionic liquid-based ferrofluids. *Colloid and Polymer Science*, 290(16), 1695–1702.
8. Laura Rodríguez-Arco, Modesto T López-López, Juan D G Durán, Andrey Zubarev & Dmitrij Chirikov. (2011). Stability and magnetorheological behaviour of magnetic fluids based on ionic liquids. *Journal of Physics: Condensed Matter*. 23(45) 455101.
9. Uhlmann, E., Spur, G., Bayat, N. & Patzwald, R. (2002). Application of magnetic fluids in tribotechnical systems. *Journal of Magnetism and Magnetic Materials*, 252, 336-340.
10. Popa, N.C., Potencz, I., Brostean, L. & Vekas, L. (1997). Some applications of inductive Transducers with magnetic fluids. *Sensors and Actuators A* 59, 197-200.
11. Goldowsky M. (1980). New methods for sealing, filtering, and lubricating with magnetic fluids. *IEEE transactions on Magnetics*, 16(2), 382-386.
12. Wu, V. M., Huynh, E., Tang, S., & Uskokovic, V. (2019). Brain and bone cancer targeting by a ferrofluid composed of super paramagnetic iron-oxide/silica/carbon nanoparticles (earthicles). *Acta Biomater*, 88, 422 - 447.

13. Scherer, C., & Antonio Martins Figueiredo Neto. (2005). Ferrofluids: properties and applications. *Braz. J. Phys.*, 35(3), 718–727.
14. Agrawal, V.K. (1986). Magnetic fluid based porous inclined slider bearing. *Wear*, 107(2), 133-139.
15. Patel, D.A., & Kataria R.C. (2022). Analysis of a double layered porous slider bearing with hyperbolic stator lubricated with ferrofluid. International *Journal of Innovation in Engineering Research & Management*, Vol 9(1), 58-68.
16. Prajapati, B. L. (1995). Magnetic fluid based porous squeeze films. *Journal of Magnetism and Magnetic Materials*, 149, 97-100.
17. Patel, K.C. (1980). The hydromagnetic squeeze film between porous circular disks with velocity slip. *Wear*, 58(2), 275-281.
18. Patel, K. C., & Gupta, J. L. (1983). Hydrodynamic lubrication of a porous slider bearing with slip velocity. *Wear*, Vol.85, 3, 309-317.
19. Salant, R. F., & Fortier, A. E. (2004). Numerical analysis of a slider bearing with a heterogeneous slip/no-slip surface. *Tribology Transactions*, Vol. 47(3), 328-334.
20. Wu, C.W., Ma, G. J., Zhou, P., & Wu, C. D. (2006). Low friction and high load support capacity of slider bearing with a mixed slip surface. *Journal of Tribology*, Vol. 128(4), 904-907.
21. Shah, R. C., & Bhat, M. V. (2002). Ferrofluid lubrication in porous inclined slider bearing with velocity slip. *International Journal of Mechanical Sciences*, Vol. 44(12), 2495–2502.
22. Ahmad, N., & Singh, J. P. (2007). Magnetic fluid lubrication of porous-pivoted slider bearing with slip velocity. *Journal of Engineering Tribology*, Vol. 221, 609-613.
23. Wang, L., Lu, C., Wang, M., & Fu, W. (2012). The numerical analysis of the radial sleeve bearing with combined surface slip. *Tribology International*, 47, 100–104.
24. Patel, J., & Deheri, G. (2014). Slip velocity and roughness effect on magnetic fluid based infinitely long bearings. *Proceedings of International Conference on Advances in Tribology and Engineering Systems,* Gujarat India, pp 97-109.
25. Shah, R.C., & Bhat, M. V. (2003). Effect of slip velocity in a porous secant-shaped slider bearing with a ferrofluid lubricant. *Fizika A-Zagreb*, 12(1), 1–8.
26. Shah, R.C., & Bhat, M.V. (2003). Ferrofluid lubrication equation for porous bearings considering anisotropic permeability and slip velocity. *Indian Journal of Engineering & Material Sciences*, 10, 277–281.
27. Shah, R.C., & Bhat, M.V. (2004). Ferrofluid lubrication of a porous slider bearing with a convex pad surface considering slip velocity. *International Journal of Applied Electromagnetics and Mechanics*, 20, 1–9.
28. Shah, R.C., & Patel, D.B. (2012). Mathematical modeling of newly designed Ferrofluid based slider bearing including effects of porosity, anisotropic permeability, slip velocity at both the ends, and squeeze velocity. *Applied Mathematics*, 2(5), 176–183.
29. Shah, R. C., & Bhat, M.V. (2004). Ferrofluid squeeze film in a long journal bearing. *Tribology international*, 37(6), 441– 446.

30. Shah, R.C., & Bhat, M.V. (2004). Anisotropic permeable porous facing and slip velocity on squeeze film in an axially undefined journal bearing with ferrofluid lubricant. *Journal of Magnetism and Magnetic Materials*, 279(2–3), 224–230.
31. Verma, P. D. S. (1986). Magnetic fluid-based squeeze film. *International Journal of Engineering Science*, 24(3), 395–401.
32. Chi, C.Q., Wang, Z. S., & Zhao, P. Z. (1990). Research on a new type of ferrofluid-lubricated journal bearing. *Journal of Magnetism and Magnetic Materials*, 85, 257–260.
33. Patel, D. A., & Kataria, R. C. (2020). Characteristics of double-porous layered slider bearing with parabolic pad stator using Ferrofluid lubricant. *International Journal of emerging Technologies*, 11(2), 1054-1060.
34. Bali, R., & Sharma, S. K. (2005). Effect of magnetic field in lubrication of synovial joints. *Tribology Letters*, Vol 19, 281-287.
35. Morgan, V. T., Cameron A. (1957). Mechanism of lubrication in porous metal bearings, conference on lubrication and wear. *London, Institution of Mechanical Engineers*, 151-157.
36. Shah, R.C., & Kataria, R. C. (2014). Mathematical Analysis of newly designed two porous layers' slider bearing with a convex pad upper surface considering slip and squeeze velocity using Ferrofluid lubricant. *International Journal of Mathematical Modelling & Computations*, 4(2), 93-101.
37. Shah, R. C., & Bhat, M.V. (2004). Ferrofluid lubrication of a slider bearing with a circular convex pad. *Journal of National Science Foundation of Srilanka*, 32(3-4), 139-148.
38. Abramovitz. S. (1955). Theory for a slider bearing with a convex pad surface; side flow neglected. The Franklin Institute Laboratories for Research and Development. *Journal of the Franklin Institute*, 259 (3), 221-233.
39. Ram, P., Kumar, Anil, K., Makinde, O. D., Kumar, P., & Joshi, V. (2017). Performance Analysis of Magnetite Nano-Suspension based porous slider bearing with varying inclination and slip parameter. *Diffusion Foundations*, vol-11, 11-21.

Appendix A

Using modified Darcy's law [34] flow of magnetic fluid in a porous matrix is given by

$$\bar{u}_i = \frac{-K_i}{\eta}\frac{\partial P_i}{\partial x} + \mu_0 \frac{K_i}{\eta}\left[M_1 \frac{\partial H_x}{\partial x} + M_2 \frac{\partial H_x}{\partial z}\right] \tag{A1}$$

$$\bar{w}_i = \frac{-K_i}{\eta}\frac{\partial P_i}{\partial z} + \mu_0 \frac{K_i}{\eta}\left[M_1 \frac{\partial H_z}{\partial x} + M_2 \frac{\partial H_z}{\partial z}\right] \tag{A2}$$

Continuity Eq. in porous region : $\frac{\partial \bar{u}}{\partial x} + \frac{\partial \bar{w}}{\partial z} = 0$ (A3)

Using Eq.s (3) and (4)

$$H_x = \frac{\partial \phi}{\partial x},\ H_z = \frac{\partial \phi}{\partial z} \text{ and } M_1 = \bar{\mu} H_x,\ M_2 = \bar{\mu} H_z\ H^2 = H_x^2 + H_z^2$$

(A4)

$$\begin{aligned} M_1 \frac{\partial H_x}{\partial x} + M_2 \frac{\partial H_x}{\partial z} &= \bar{\mu} \left(\frac{\partial \phi}{\partial x} \frac{\partial^2 \phi}{\partial x^2} + \frac{\partial \phi}{\partial z} \frac{\partial^2 \phi}{\partial x \partial z} \right) \\ &= \frac{\bar{\mu}}{2} \frac{\partial}{\partial x} \left\{ \left(\frac{\partial \phi}{\partial x} \right)^2 + \left(\frac{\partial \phi}{\partial z} \right)^2 \right\} \\ &= \frac{\bar{\mu}}{2} \frac{\partial}{\partial x} \left\{ \left(H_x^2 + H_z^2 \right) \right\} \\ &= \frac{\bar{\mu}}{2} \frac{\partial H^2}{\partial x} \end{aligned}$$

(A5)

And $M_1 \frac{\partial H_x}{\partial x} + M_2 \frac{\partial H_x}{\partial z} = \frac{\bar{\mu}}{2} \frac{\partial H^2}{\partial x}$

$$\begin{aligned} \bar{u}_i &= \frac{-K_i}{\eta} \frac{\partial P_i}{\partial x} + \frac{K_i \mu_0 \bar{\mu}}{2\eta} \frac{\partial H^2}{\partial x} \\ &= \frac{-K_i}{\eta} \frac{\partial}{\partial x} \left(P_i - \frac{1}{2} \mu_0 \bar{\mu} H^2 \right), \\ \bar{w}_i &= \frac{-K_i}{\eta} \frac{\partial P_i}{\partial z} + \frac{K_i \mu_0 \bar{\mu}}{2\eta} \frac{\partial H^2}{\partial z} \\ &= \frac{-K_i}{\eta} \frac{\partial}{\partial z} \left(P_i - \frac{1}{2} \mu_0 \bar{\mu} H^2 \right) \end{aligned}$$

(A6)

which represent Eq.s (16) and (17) of present study.

We assume that the applied magnetic field has the components

$$H_x = H(x)\cos\phi,\ H_y = H(y)\sin\phi \text{ and } H^2 = H_x^2 + H_y^2,\ \frac{\partial H^2}{\partial y} = 0$$

.

Appendix B

Calculation of maximum magnetic field strength *K*

From Eq. (3), $H^2 = Kx(A - x)$, attains maximum at $x = A/2$ giving

$$H_{Max}^2 = 0.56 \times 10^{-2} K \text{ for } A=0.15,$$

For $K = \frac{10^8}{0.56}$, $H \approx O(10^3)$ or $O(H) \approx 3$, where *O* indicates the order.

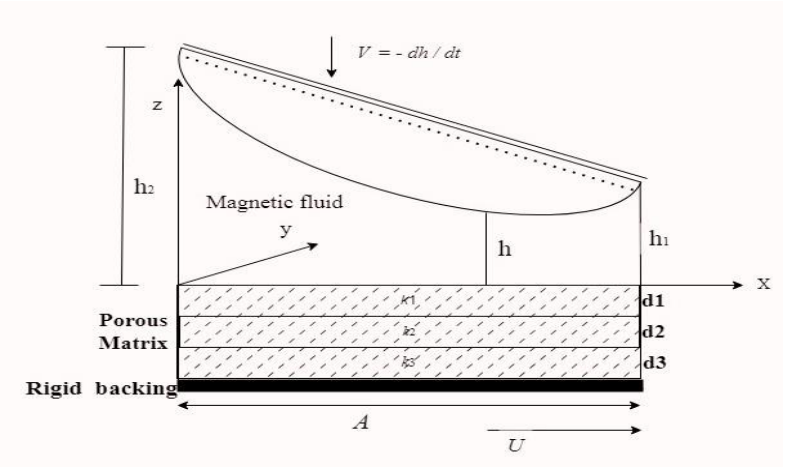

Fig. 1 Slider bearing with a convex pad

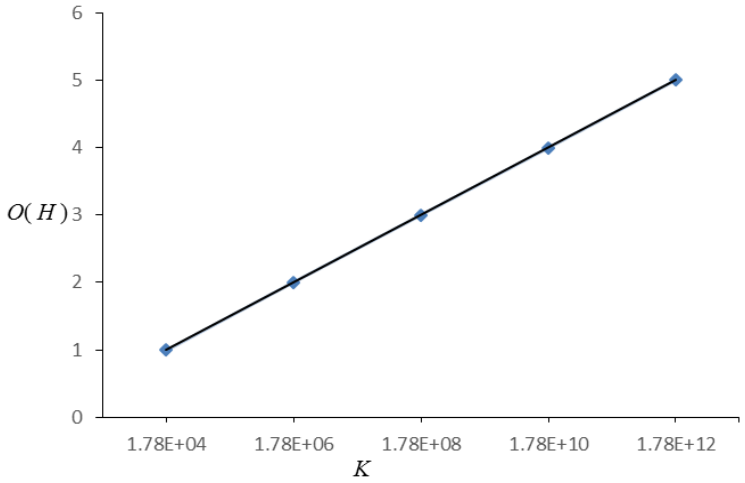

Fig. 2 Order of magnetic field strength *O*(*H*) for different values *of K*

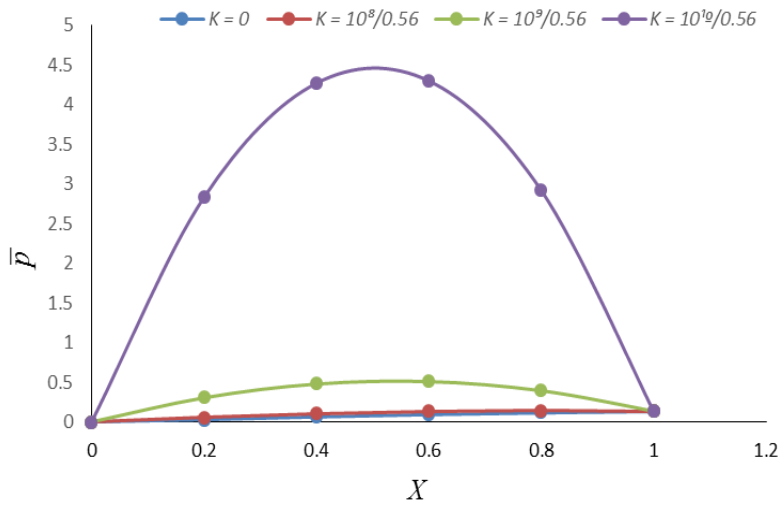

Fig. 3 $\bar{p}$ for different values of non-dimensional parameter *X* using different values of *K*

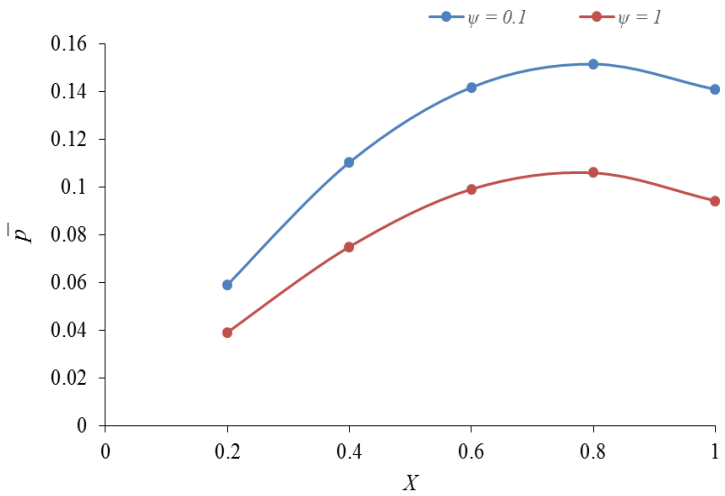

Fig. 4 Effect of the permeability parameter ψ on the non-dimensional film pressure $\bar{p}$

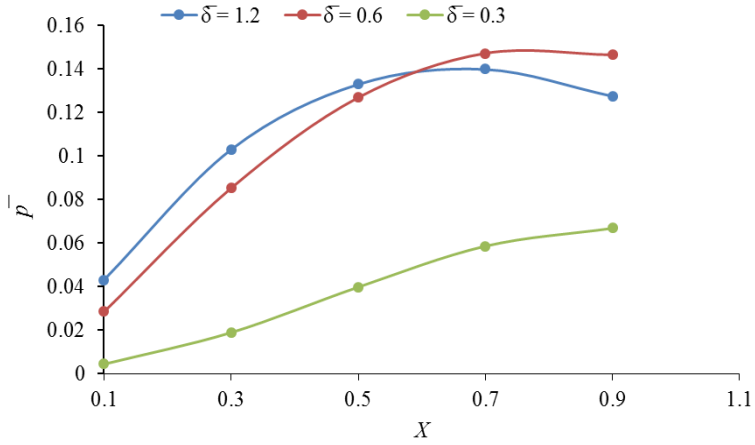

Fig. 5 $\bar{p}$ verses X with non-dimensional parameter $\bar{\delta}$

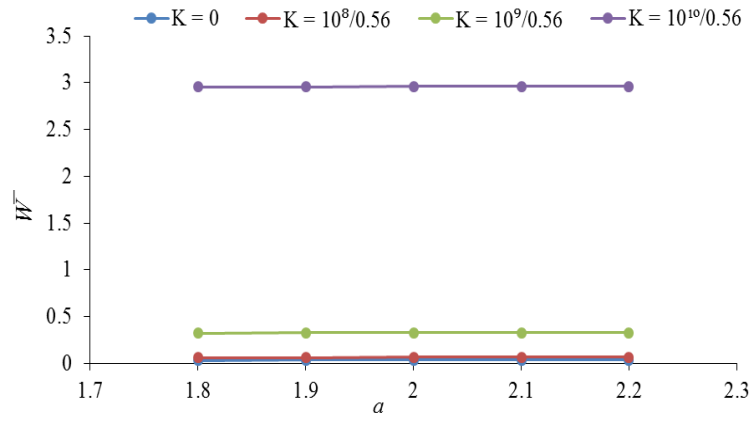

Fig. 6 Variation in $\bar{W}$ verses a, for different values K

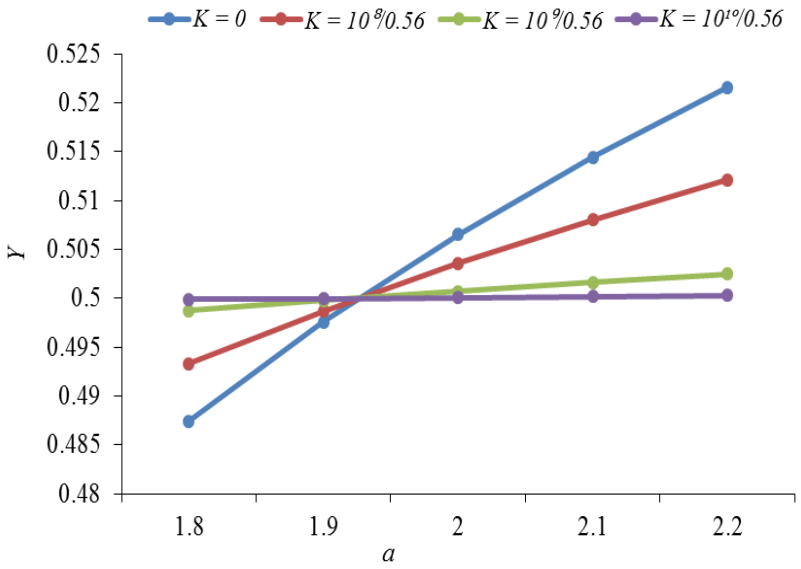

Fig. 7 Variation in $\overline{W}$ verses a for different values K

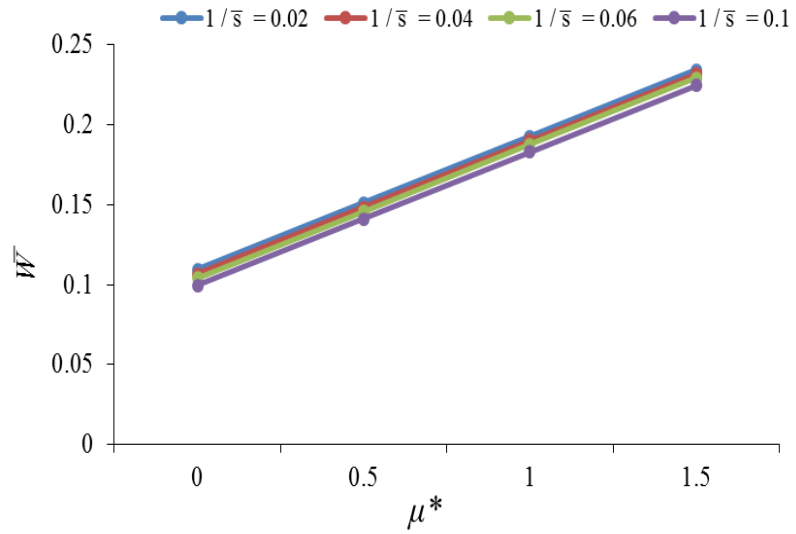

Fig. 8 Variation in $\overline{W}$ verses μ^* for various values of slip parameter $1/\bar{s}$

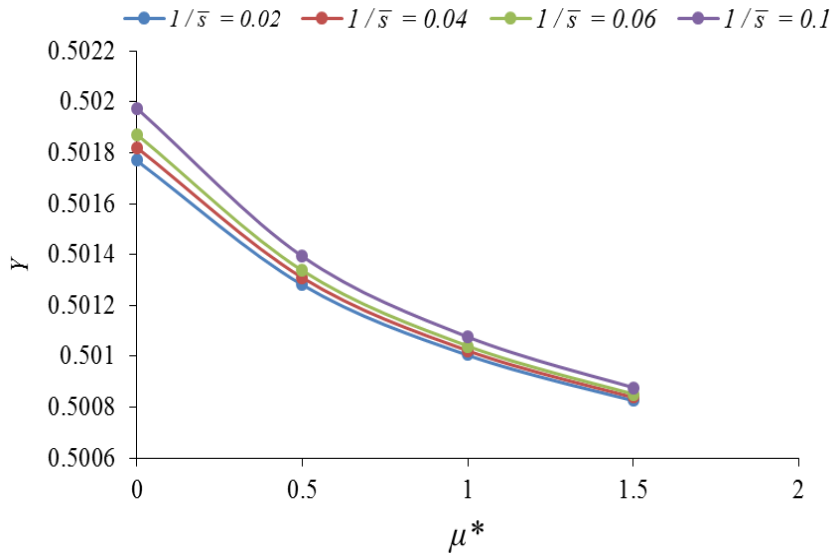

Fig. 9 Variation in Y verses μ^* for various values of slip parameter $1/\bar{s}$

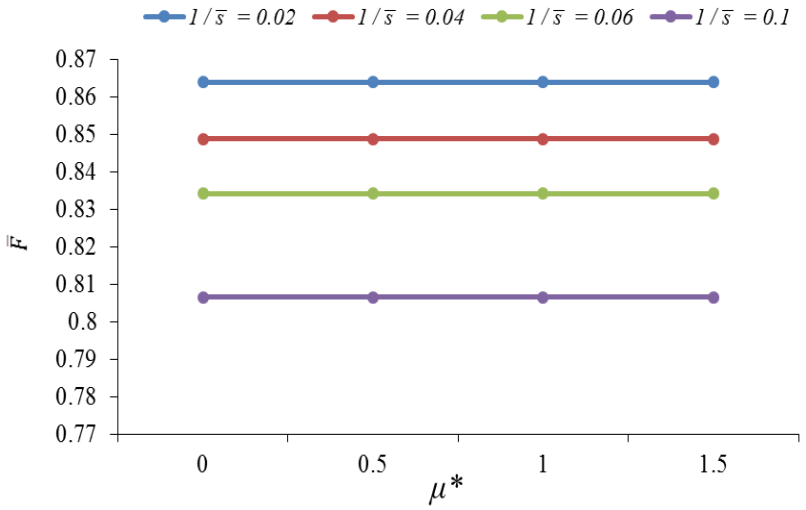

Fig. 10 Variation in $\bar{F}$ verses μ^* for various values of slip parameter $1/\bar{s}$

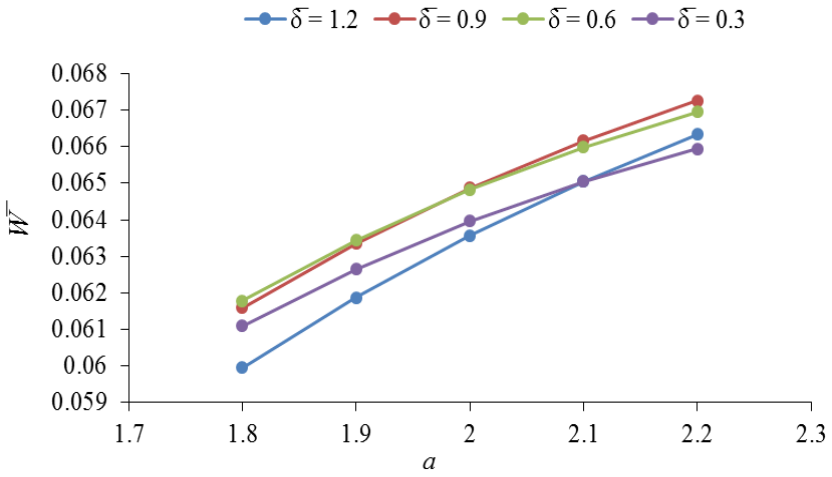

Fig. 11 Variation in $\bar{W}$ verses a for various values of $\bar{\delta}$

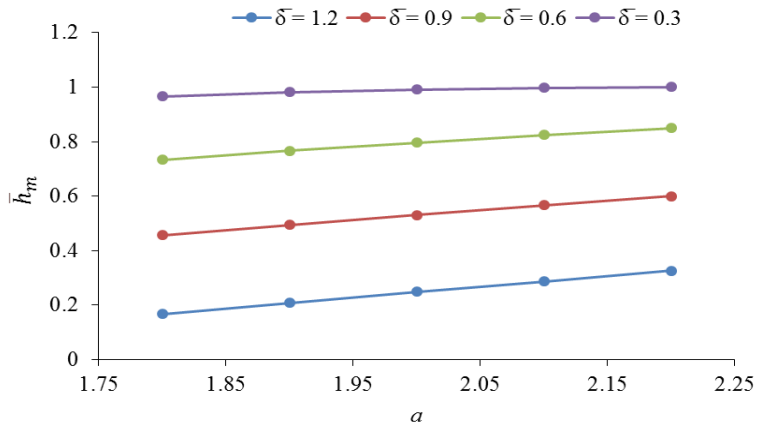

Fig. 12 Variation in $\bar{h}_m$ verses a for various values of $\bar{\delta}$

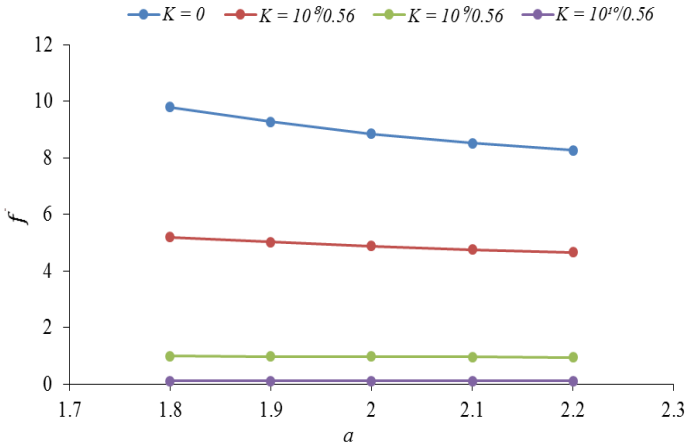

Fig. 13 Variation in $\bar{f}$ verses a for various values of K

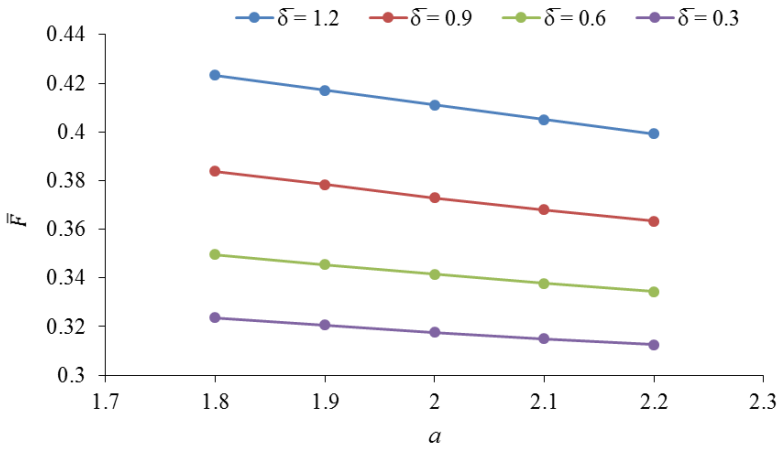

Fig. 14 Variation in $\bar{F}$ verses a for various values of $\bar{\delta}$

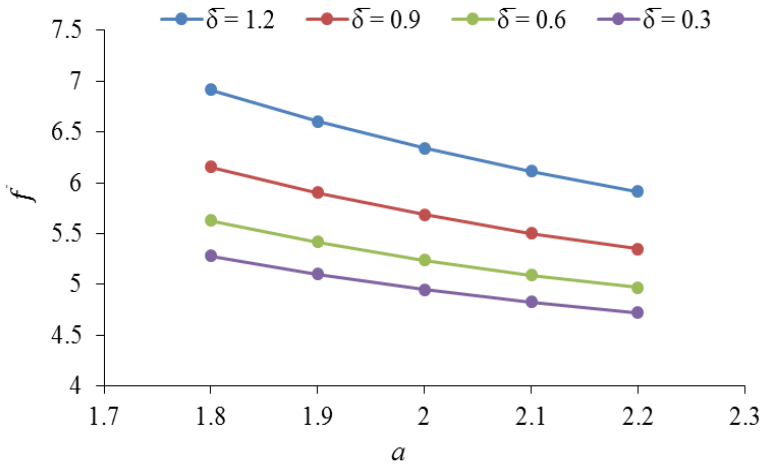

Fig. 15 Variation in $\bar{f}$ verses a for various values of $\bar{\delta}$